Talanta 85 (2011) 298–303

Contents lists available at ScienceDirect

Talanta

journal homepage: www.elsevier.com/locate/talanta

UV-ablation nanochannels in micro/nanofluidics devices for biochemical analysis

Chen Wang[a], Jun Ouyang[a], Hong-Li Gao[a], Heng-Wu Chen[b], Jing-Juan Xu[a], Xing-Hua Xia[a,*], Hong-Yuan Chen[a]

[a] Key Laboratory of Analytical Chemistry for Life Science, School of Chemistry and Chemical Engineering, Nanjing University, 22 Hankou Road, Nanjing, Jiangsu 210093, China
[b] Institute of Microanalytical Systems, Department of Chemistry, Zhejiang University, Hangzhou 310058, China

ARTICLE INFO

Article history:
Received 20 January 2011
Received in revised form 13 March 2011
Accepted 24 March 2011
Available online 6 April 2011

Keywords:
UV-ablation
Size-tunable
Micro/nanofluidics
Protein concentration
Bioanalysis

ABSTRACT

This paper presents a simple and cost-effective UV-ablation technique for fabrication of size-tunable nanofluidics devices via photochemical decomposition reaction. UV-irradiation through a PET photomask results in continuous decomposition of poly(carbonate) (PC), forming nanochannel and carboxyl groups on the surface of the etched PC. This photochemical decomposition process occurs at molecular scale, therefore, the depth of nanochannels can be controlled at nanometer level. The etching rate is estimated to be ca. 0.015 nm s^{-1}. To demonstrate the potential application of the present UV-ablation technique, a nanochannel was fabricated and integrated with microchannels to form a micro/nanofluidics chip for protein concentration. Using this device, about 10^3–10^5 fold protein concentration can be achieved within 10 min. The present approach offers a simple and practical solution to fabricate nanofluidics devices at low-cost, and the resulting device could provide ideal platforms for μTAS towards various applications in biology and chemistry.

1. Introduction

In recent years, interests on microfluidics devices for analytical chemistry or biochemistry have been dramatically increasing [1]. With the fast progress in the fields of microfluidics and nanotechnology, further downsizing fluidic channels to nanometer scale can further reduce costs, processing time, amount of reagents necessary for assay as compared with microfluidics systems; therefore, this field of nanofluidics is growing rapidly in the recent years.

Nanofluidics enable us to observe flow behaviors of fluids in nanostructures with at least one of the dimensions falling in the nanosize range, i.e., several to one hundred nanometers [2]. Nanostructures promise various applications in chemical and biological analysis. For example, nanostructures integrated to microfluidics form micro/nanofluidics devices which have been successfully used for protein concentration [3], enzyme kinetics assay [4], cell assays [5], single DNA analysis [6], and immonoassay [7]. In our previous work, we have reported on integration of nanostructures including porous anodic alumina membrane [8], single nanochannel [9,10] with microfluidics for protein concentration and enzyme kinetics assay.

Up to now, various methods have been proposed to fabricate nanofluidics devices and the progress of this area has been already reviewed recently [11]. In the fabrication of nanostructures in microfluidics devices, bulk machining [12], surface machining [13], and mold machining [14], have been usually used. For example, in the bulk machining process, nanochannels on various substrates can be easily fabricated by using photolithographic techniques. This method is simple in principle, and is suitable for mass production. However, most lithographic methods are expensive. Furthermore, in order to get smaller size channels, many sophisticated techniques including electron-beam lithography and proton beam writing are required. In the case of surface nanomachining method, which is also called sacrificial layer technology, a bottom layer is first deposited on a wafer. Then, a sacrificial layer is deposited on the bottom layer, which is subsequently etched prior to the formation of the final nanochannel. This method requires relatively long time to remove the sacrificial layer. In the mold machining method, a polydimethylsiloxane (PDMS) layer is directly casted onto a mold with inverse shape of the desired structures to form the nanochannels. Although this method is simple and has been widely used in mass production, it requires the electron beam lithography and focused ion beam milling techniques to fabricate high-resolution nanoscale templates, which will certainly lead to a higher cost. Therefore, the fundamental challenges imposed on fabricating nanofluidics devices are to develop simple, low-cost and rapid fabrication techniques of nanostructures. The developed technique should also be accessible to normal laboratories.

Polymeric materials have been widely used in micro/nanofluidics devices fabrication due to their distinct advantages of low cost, ease of fabrication, and higher flexibility over silicon, glass and quartz. The typical fabrication techniques

* Corresponding author. Tel.: +86 25 83597436; fax: +86 25 83685947.
E-mail address: xhxia@nju.edu.cn (X.-H. Xia).

0039-9140/$ – see front matter © 2011 Elsevier B.V. All rights reserved.
doi:10.1016/j.talanta.2011.03.057

on organic polymers mainly rely on hot embossing or imprinting, injection molding, laser ablation, soft lithography, or X-ray photolithography. However, these methods usually require specialized and expensive equipments, and are not commonly accessible to most laboratories. Recently developed photochemical etching technique is a simple and efficient means for micro-/nano-scale wells fabrication and biomolecules patterning [15–18]. Tertiary-amine-terminated poly(ethylene terephthalate) (PET) surface has been synthesized by using a UV-light induced surface aminolysis reaction [16]. Thus, biomolecules such as proteins can be patterned on the light-irradiated areas via the electrostatic interactions. Soper [17] and Chen [18] also demonstrated approaches for efficient patterning of biological molecules and metal films on poly(carbonate) (PC) surfaces through photochemical reaction. We carefully studied this photochemical etching process and found that: (1) the photochemical etching reaction can continuously decompose the polymer at molecular level. Therefore, the etching depth can be controlled at nanoscale by properly choosing UV-irradiation time and UV-light intensity. During the process of UV-light irradiation, the photon energy of UV-light excites and dissociates most of the chemical bonds of the polymer, resulting in layer-by-layer ablation of the polymer. This phenomenon is similar to the laser ablation, thus we rename this process as UV-ablation in the present work. (2) The formed carboxyl groups resulting from UV-light photochemical decomposition can increase the surface charge of the resultant micro/nanochannels, improving the electroosmosis force. (3) The covalently bounded biomolecules would make the electroosmotic flow more stable, which is very important for liquid manipulation on μTAS. (4) The UV lamp does not irradiate infrared ray, accordingly, thermal damage due to heat generation to the polymer surface is negligible. This is strictly important for fabricating nanochannels on polymer surfaces in the followed assembly process. (5) This method is accessible to normal laboratories. Therefore, we believe this simple UV photochemical decomposition method should be an alternative, facile and low cost technique for fabricating nanochannels on polymer chips and will certainly promote progress of the nanofluidics research area.

In this work, learned from these advantages of photochemical etching technique, we use this UV-ablation technique to fabricate depth-tunable nanochannels and a micro/nanofluidics device for protein concentration, in which a single nanochannel was integrated on a microfluidics device (Fig. 1). The single nanochannel was achieved by exposing a PC substrate to UV-irradiation for 20 min at a lamp-to-plate distance of 2.0 cm. The depth of nanochannel is estimated as ca. 18 nm according to the etching rate. Using this device, about 10^3–10^5 fold protein concentration can be achieved within 10 min.

In our previous work [9], an electric field breakdown technique has been proposed to fabricate nano fissures. Although the resultant nanofluidics can be successfully used to concentrate proteins carrying the same charges as the nanochannel surface, the control of channel size using this method is impossible. In addition, it is impossible to fabricate single nanochannel with designed size. In another report [10], the nanochannel was fabricated according to the method described previously [19], and the work was focused on the study of homogeneously enzymatic reaction kinetics of the concentrated enzyme. Similarly, the nanochannel cannot be fabricated in a controllable way. As compared to the nanochannels fabrication methods in our previous reports and others [9,10,19], the present UV photochemical decomposition method for nanochannels fabrication shows many advantages as described above. Besides, the present method provides us the possibility to fabricate nanochannels with tunable size. We believe that the present facile fabrication method offers a simple and practical solution to fabricate nanofluidics devices at low-cost, and the resulting devices could provide platforms for μTAS towards various applications in biology and chemistry.

2. Experimental

2.1. Material and methods

Phosphate buffer (PBS, pH 7.0, 10 mM) solution was used as the buffer system. Fluorescein isothiocyanate labelled dog serum albumin (FITC-DSA), rhodamine B, and fluorescein (FITC) were obtained from Sigma and used as received. All solutions were kept in a freezer to prevent deterioration. All liquid samples were prepared from deionized water (18 MΩ cm, PURELAB Classic, PALL, USA) and filtered through a 0.22 μm syringe filter to remove particulates prior to use.

2.2. Micro/nanofluidics chips fabrication

The whole fabrication process of micro/nanofluidics device for protein concentration is schematically shown in Fig. 1. Briefly, there are three steps including (1) nanochannel formation on PC sheet by UV-ablation, (2) microchannel formation on a PDMS slab, and (3) final formation of a PC/PDMS micro/nanofluidics chip.

For nanochannel fabrication, a PC surface is exposed to 254-nm UV-light with a power density of 5 mW cm^{-2} in a O_2 containing environment (e.g., air) using a commercially available poly(ethyleneterephthalate) (PET, DIKA Official Limited Company, Suzhou, China) film as the photomask since the PET film can hardly transmit UV-light with wavelengths ranging from 200 to 285 nm [20]. The width and length of nanochannels on PET were made with a sharp knife. For fabrication of microchannels, a PDMS layer was directly casted over an SU-8 photoresist mold deposited on a silicon substrate fabricated by photolithography as previously described [10]. Then, the PDMS slab with microchannels and reservoirs (m, n, p, q) was reversibly sealed to the etched PC plate

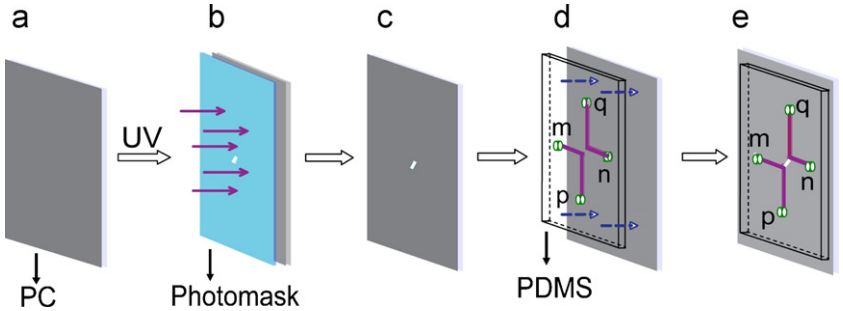

Fig. 1. Schematic layouts of the micro/nanofluidics chips fabrication processes. (a) Native PC plate; (b) UV-lights irradiated PC under a PET photomask; (c) pattern transfer of the photomask onto PC surface; (d) sealing PDMS with microchannels and four reservoirs (m, n, p, q) to PC with nanochannel reversibly; (e) formation of the final micro/nanofluidics chip for protein concentration. Total length p–q = 16 mm.

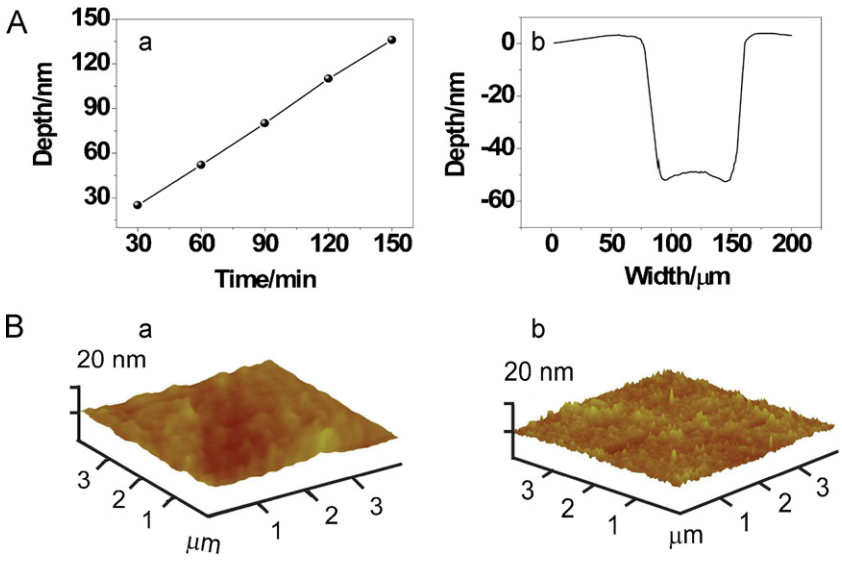

Fig. 2. (A, a) Plot of channel depth as function of UV-irradiation time with plate-to-lamp distance 2 cm and 254 nm UV-irradiation. (A, b) Depth profile of the channel area on the PC surface after 60-min UV-irradiation through a PET photomask. (C) AFM images of a native PC surface (B, a) and 120-min UV-irradiated PC surface (B, b).

with nanochannel to form a complete micro/nanofluidics chip. This assembly process similar to ones reported previously [10,19] produces a "reversible" bonding between PDMS slab and PC substrate that can be easily peeled apart. In our measurements, leakage of fluids or formation of bubbles in channels is not observed. The reversible assembly avoids channels collapsing usually observed in conventional thermal bonding process. In the present work, the height of the nanochannel is about 20 nm, the width 200 μm, and the length 100 μm. The dimensions of the microchannel are respectively 18 μm in height, 100 μm in width. The total length of the micro/nanofluidics chip (p–q) is 16 mm long.

2.3. Characterization of the etched nanochannel

The depth of etched nanochannels was measured on a profilometer (Dektak 3, Veeco Inst Inc., USA). The morphologies of the nanochannels were characterized using an atomic force microscopy (AFM, Picoforce, Veeco Inst Inc., USA).

2.4. Instrumentation and electrical setup

Fluorescence detection and microscopic investigations were performed using an inverted fluorescence microscope (Nikon, Ti-U, Japan) equipped with a highly sensitive CCD color video camera (S45, Canon, Japan). NIS-elements BR 2.30 software (Nikon) was used for camera control and image processing. A laboratory-made high voltage power supply (0–5000 V) was used to apply electric fields to the microchannels through platinum electrodes placed in reservoirs. The applied voltage can be automatically controlled by a personal computer via an AD/DA converter, and the current is monitored in real time and the corresponding data can be saved in text files.

2.5. Proteins concentration procedures

In order to investigate the protein enrichment capacity of the micro/nanofluidics device fabricated in this work, solutions of FITC-DSA in 10 mM PBS (pH 7.0) were used as demonstration. The micro/nanofluidics chip for protein enrichment is schematically shown in Fig. 1e. The enrichment procedures have been described previously [9,10]. Briefly, running buffer was first introduced in all reservoirs to fill all the channels by squeezing slightly the buffer solution in the channels. Then, FITC-DSA solution was introduced into the protein reservoir. Protein electrokinetic enrichment experiments were carried out by a laboratory-made high voltage power supply. Voltage was applied on the protein reservoir, with the waste reservoir grounded and the other reservoirs floating. To prevent nonspecific deposition of protein onto the PDMS and PC surfaces, bovine serum albumin (5% solution in 10 mM PBS (pH7.0)) was first filled in the microchannel for several hours for each new micro/nanofluidics chip and followed by flushing with buffer solution until the current of the power supply levelled off.

3. Results and discussion

3.1. Formation of nanochannel

UV-light irradiation through the PET photomask (200 μm wide) decomposes the PC continuously, resulting in the formation of nanochannel and carboxyl groups on the surface of the etched PC, while the properties and morphology of the masked area do not change. A profilometer was used to characterize the morphology of the nanochannel fabricated by 60 min UV-irradiation. It is found that the etched nanochannel is trapezoidal with smooth corners, as shown in Fig. 2A, b. UV-ablation does not produce obvious widening effect in lateral size to the formed nanochannel as compared to the PET photomask structure. However, edge effect in UV-ablation process is observable as indicated by the arched bottom profile, which is probably due to accelerated diffusion of oxygen at the edge area or the unparallel UV-lights intensity. By controlling the UV-irradiation time, channel depths from 0 to 140 nm can be fabricated within irradiation time of 150 min at a lamp-to-plate distance of 2.0 cm (Fig. 2A, a). The etching rate is estimated to be about 0.015 nm s^{-1}. Interestingly, UV-ablation results in a smoothing effect to the PC surface. As shown by the atomic force microscopic images in Fig. 2B, after 120 min UV-irradiation, the PC surface becomes smoother as compared to the native PC surface. This phenomenon may imply that the photochemical reaction occurs heterogeneously and starts at defects, e.g., roughened sites. In addition, the UV lamp does not irradiate infrared ray, accordingly, thermal damage due to heat formation to the polymer surface is negligible. This is strictly important for fabricating nanochannels on polymer surface in the followed assembly process.

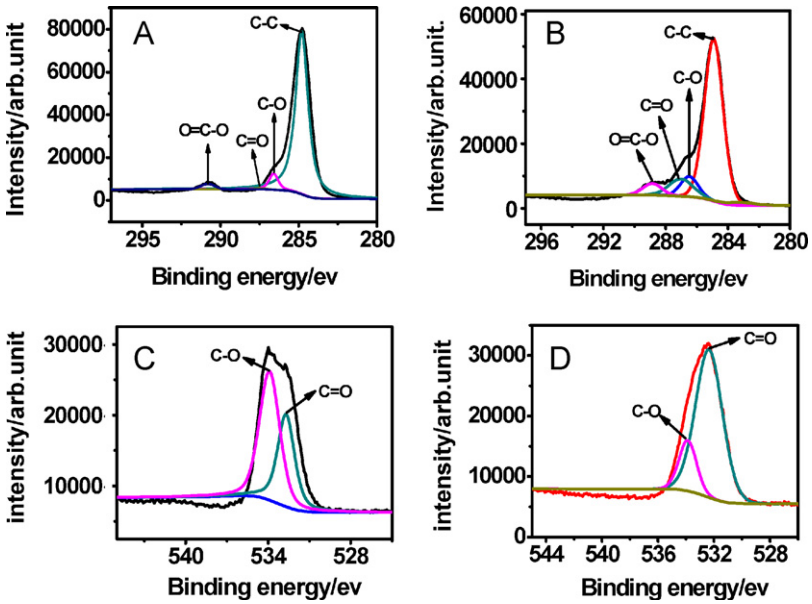

Fig. 3. XPS spectra of UV-irradiated PC substrates. C 1s (A) and O 1s spectra (C) of a native PC; C 1s (B) and O 1s (D) spectra of the PC irradiated for 120 min.

Poly(carbonate) (PC) structure contains an ester and a carbonate bond in each repeat unit. The photon energy of UV-light is high enough and can excite and dissociate most of the chemical bonds to form free radicals at the polymer surface. The radicals readily react with activated oxygen species generated through the photo excitation of oxygen molecules in the air, resulting in the formation of carboxyl groups [21]. In addition, hydrolysis of the carbonate bond generates unstable carbonic acid, which further decomposes to CO_2 [22]. The gaseous decomposition products easily release from the PC surface, leaving channels with height at nanometer scale on the polymer surface. Therefore, the release of gaseous decomposition products from the ester group results in the formation of nanochannel on polymer surface. The shape of these nanochannels is determined by the structure of photomask and UV-irradiation time. Furthermore, this conversion of polymer into gaseous product does not contaminate the polymer surface. From Fig. 2B, it can be seen that the PC surface becomes smoother as compared to the native PC surface after UV-irradiation. This photochemical decomposition process occurs at molecular scale, something like molecular epitaxy process. Therefore, depth of the nanochannel can be controlled at nanometer level as expected.

In order to understand the photochemical reaction occurring on the PC surface, C 1s and O 1s X-ray photoelectron spectroscopic (XPS) spectra of PC films before and after UV-irradiation were measured. The results are shown in Fig. 3 and detailed analysis data are listed in Table 1.

Table 1
Chemical compositions of the PC substrates before and after 120 min UV-irradiation.

	Native PC			UV irradiated PC		
	Position (eV)	Fwhm (eV)	Area ratio (%)	Position (eV)	Fwhm (eV)	Area ratio (%)
C 1s components						
C–C	284.9	1.05	86.81	284.9	1.43	71.06
C–O	286.5	0.81	9.41	286.5	1.43	15.23
C=O	287.4	0.34	0.75	287.3	2.62	7.21
O=C–O	290.7	1.01	3.03	288.9	2.55	6.51
O 1s components						
C=O	532.0–532.6	1.51	38.58	532.2	2.04	64.53
C–O	533.9	1.94	61.42	533.7	1.90	35.47

The typical C 1s XPS spectrum (Fig. 3A) of a native PC consists of three components centered at binding energies (BEs) of 284.9, 286.5, 287.4, and 290.7 eV, respectively corresponding to C–C, C–O, C=O, and O=C–O groups [16,21]. After UV irradiation for 120 min, the markedly different C 1s XPS spectrum is obtained (Fig. 3B). It consists of four components centered at BEs of 284.9, 286.5, 287.3, 288.9 eV, which correspond to C–C, C–O, C=O, and O=C–O groups, respectively [16,21]. It is noteworthy that the band intensity for the C=O groups increases from 0.75% to 7.21% after the UV-irradiation, the relative intensity of the C–C groups decreases from 86.81% (native PC) to 71.06% (UV-irradiated PC); while the intensity for the O=C–O group increases considerably from 3.03% (native PC) to 6.51% (irradiated PC). The O 1s XPS spectrum (Fig. 3C) of the native PC consists of two components centered at BEs of 532.0–532.6, and 533.9 eV, corresponding to C–O and O=C–O groups, respectively. After UV-irradiation, the relative intensity of the C–O groups decreases from 61.42% (native PC) to 35.47% (irradiated PC); while the intensity of the C=O group increases markedly from 38.58% (native PC) to 64.53% (irradiated PC) as indicated in Fig. 3D. The results demonstrate that photochemical decomposition of ester side groups in the PC unit occurs.

3.2. Electroosmotic flow (EOF) measurements

The electroosmotic flow (μ_{EOF}) was determined with the elution time of a neutral marker hydrogen peroxide [10]. The neutral marker is carried through the channel under the action of only electroosmotic flow and the μ_{EOF} can thus be evaluated using Eq. (1), where L is the length of separation channel, V is the applied separation voltage, and t is the migration time of the neutral marker.

$$\mu_{EOF} = \frac{L^2}{Vt} \quad (1)$$

For nanofluidics devices fabricated on polymer materials, electroosmotic flow is often slow due to the low surface charge density. In the present approach, carboxyl groups generated simultaneously as the nanochannel forms. Therefore, the channel surface exhibits substantially higher water wettability (Fig. S1) and electroosmotic flow (Table 2), which is crucial for liquid manipulation in nanochannels. All these advantages promise the present method

Table 2
The μ_{EOF} values for the glass/PDMS microchip, PC/PDMS microchip and PC/PDMS nanochip.

Types of chips		μ_{EOF}/cm^2 V^{-1} s^{-1}	Standard deviation
Glass/PDMS	Microfluidics chip	2.48×10^{-4}	5.8%
PC/PDMS (pristine)	Microfluidics chip	1.77×10^{-4}	6.4%
PC/PDMS (90 min irradiation)	Microfluidics chip	2.26×10^{-4}	6.1%
	Nanofluidics chip	7.5×10^{-5}	7.2%

for fabrication of polymeric micro/nanofluidics devices for bioanalysis.

3.3. Enrichment capacity of the micro/nanofluidics chip

The protein concentration experiments were first operated on the device illustrated in Fig. 1A. To prevent nonspecific binding of proteins onto PDMS and PC surface, bovine serum albumin was introduced into the microchannel and incubated for several hours for each new micro/nanofluidics chip. Then, they were flushed thoroughly with buffer solution. Upon application of a 400 V high voltage to the protein reservoir (anode) and waste reservoir (cathode), the negatively charged fluorescein isothiocyanate labelled dog serum albumin (FITC-DSA) sample is concentrated at the anodic electrode side in front of the nanochannel. Three different initial concentrations (0.1, 1.0, 10 μg ml^{-1}) samples were used to study the enrichment effect. Fig. 4B shows the plot of concentration of FITC-DSA as a function of enrichment time at a voltage of 400 V. The inset shows the enlarged plot of 0.1 μg ml^{-1} FITC-DSA. From the change of fluorescence intensity, it can be known that at the first 150 s enrichment time, the enrichment effect is not clear. This time period is mainly used to drive samples in the microchannel. Increasing the time further results in rapid enrichment of FITC-DSA in front of the nanochannel and soon reaches saturation. The proteins enrichment results indicate that the present micro/nanofluidics chip has a perfect protein enrichment capacity which is comparable to previous reports obtained on various nanofluidics devices [9,10,19].

The concentration mechanism can be explained by the exclusion-enrichment effect (EEE) [9,10,19]. When buffer is filled into the channels, an electrical double layer (EDL) forms immediately at the liquid–solid surface. For a typical buffer solution with ionic strengths from 1 to 100 μM, the EDL thickness ranges from 1 to 10 nm. Since this thickness is neglectable in micrometers scale, the EDL has little influence on the transport of charged analytes in microchannels. However, when the channel size shrinks to nanometer scale, the transport of charged analytes will differ significantly from that in microchannels for the thickness of EDL is comparable to the nanochannel radius. The potential within the nanochannel is dependent on the surface charge of the channel wall, negative for positively charged surface, and vice versa. Therefore, co-ions (the same charge as the surface carrying) can pass through the nanochannel and the counter-ions are excluded due to the electrostatic interactions. In the present case, the nanochannel wall carries negative charges, therefore, anions will be concentrated in front of the nanochannel, whereas cations (or counterions) can transport through it.

To confirm the EEE mechanism in our system, additional experiments were performed. Small molecular probes, rhodamine B and fluorescein (FITC), were also used to investigate the concentration mechanism. In the present buffer system used (pH 7.0),

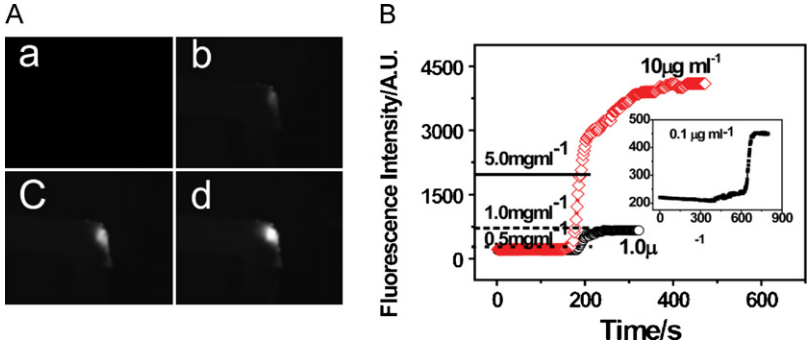

Fig. 4. (A) Time sequence photo images (a–d) of 10 μg ml^{-1} FITC-DSA in 10 mM PBS (pH 7.0) in the micro/nanofluidics device. Images were taken after applying a voltage of 400 V between proteins reservoir and waster reservoir for 0, 180, 200, 300 s, respectively. (B) Plot of FITC-DSA concentration from three initial concentration samples at voltage of 400 V as a function of enrichment time. The inset shows the enlarged plot of 0.1 μg ml^{-1} FITC-DSA.

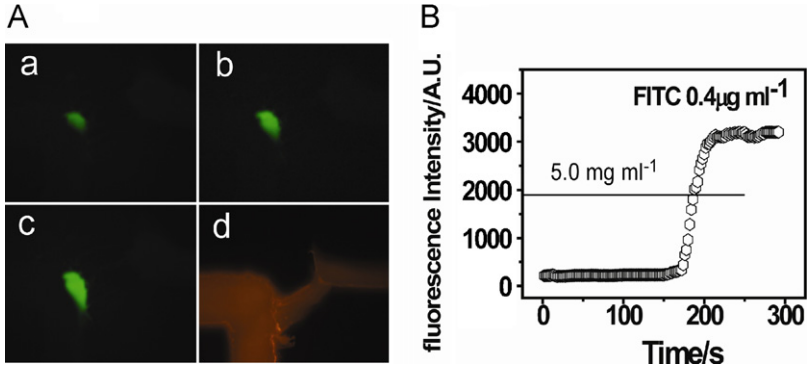

Fig. 5. (A) Time sequence photo images (a–c) of 0.4 μg ml^{-1} FITC in 10 mM PBS (pH 7.0) in the micro/nanofluidics device. Images were taken after applying a voltage of 400 V between the feeding reservoir and waster reservoir for 180, 200, 300 s, respectively. The image (d) from 0.4 μg ml^{-1} rhodamine B was collected at 300 s under the same conditions as FITC enrichment experiments. (B) Plot of FITC concentration at voltage of 400 V as a function of enrichment time.

rhodamine B is positively charged and fluorescein is negatively charged. According to the EEE mechanism, anionic analytes cannot pass through the nanochannels. This is further confirmed by the experimental results shown in Fig. 5. Rhodamine B can easily pass through the nanochannel and no concentration occurs; while the positively charged fluorescein cannot pass through the nanochannels and is thus accumulated in front of nanochannels of the micro/nanofluidics devices. Based on this phenomenon, we successfully established a label-free DNA sensor using nanochannels [23].

4. Conclusion

In summary, we have presented a simple and cost-effective method for fabrication of nanofluidics devices based on photochemical decomposition reaction. This technique is simple, fast and low-cost, and is accessible to most laboratories. Obviously, the present approach offers many obvious advantages over other approaches. The photochemical decomposition reaction occurs at molecular level, thus, it allows facile control of the channel depth at nanoscale level. The carboxyl groups generated from photochemical reaction considerably improve the wettability and electroosmosis of the channels, and can be further used to pattern biological molecules. The observed smoothing effect of the UV-ablation method would be an additional advantage being critical to nanofluidics devices fabrication. Our results have shown that the fabricated nanofluidics device can be successfully used for proteins concentration. These results suggest that nanofluidics devices fabricated using the UV-ablation method are specially promising to the study of chemical and biological reactions on nanoscale. We expect that the present fabrication method and the resulting nanostructures with functionalized surfaces could provide new platforms for nanofluidics development towards various applications in biology and chemistry such as concentrations, filtrations, heterogeneous enzymatic reaction kinetics, immunoassays, and biosensors.

Acknowledgements

This work was supported by the Grants from the National 973 Basic Research Program (2007CB714501, 2007CB936404), the National Natural Science Foundation of China (20890020, 20975047, 21035002), the National Science Fund for Creative Research Groups (20821063), the Ministry of Education of China (200802840012) and the Natural Science Foundation of Jiangsu province (BK2010009).

Appendix A. Supplementary data

Supplementary data associated with this article can be found, in the online version, at doi:10.1016/j.talanta.2011.03.057.

References

[1] (a) J. Atencia, D.J. Beebe, Nature 437 (2005) 648–655;
(b) A. Gunther, K.F. Jensen, Lab Chip 6 (2006) 1487–1503;
(c) H. Song, R.F. Ismagilov, J. Am. Chem. Soc. 125 (2003) 14613–14619.
[2] A. Patrick, T.N. Nam, Anal. Chem. 80 (2008) 2326–2341.
[3] (a) H. Cui, K. Horiuchi, P. Dutta, C.F. Ivory, Anal. Chem. 77 (2005) 1303–1309;
(b) D. Akin, H. Li, R. Bashir, Nano Lett. 4 (2004) 257–259.
[4] J.H. Lee, Y.A. Song, S.R. Tannenbaum, J. Han, Anal. Chem. 80 (2008) 3198–3204.
[5] J.H. Lee, B.D. Cosgrove, D.A. Lauffenburger, J. Han, J. Am. Chem. Soc. 131 (2009) 10340–10341.
[6] P. Sivanesan, K. Okamoto, D. English, C.S. Lee, D.L. Devoe, Anal. Chem. 77 (2005) 2252–2258.
[7] T. Endo, K. Kerman, N. Nagatani, H.M. Hiepa, D. Kim, Y. Yonezawa, K. Nakano, E. Tamiya, Anal. Chem. 78 (2006) 6465–6475.
[8] (a) J.H. Yuan, W. Chen, R.J. Hui, Y.L. Hu, X.H. Xia, Electrochim. Acta 51 (2006) 4589–4595;
(b) W. Chen, J.H. Yuan, X.H. Xia, Anal. Chem. 77 (2005) 8102–8108;
(c) S.J. Li, C. Wang, Z.Q. Wu, J.J. Xu, X.H. Xia, H.Y. Chen, Chem. Eur. J. 16 (2010) 10186–10194;
(d) W. Chen, Z.Q. Wu, X.H. Xia, J.J. Xu, H.Y. Chen (Eds.), Angew. Chem. Int. 49 (2010) 7943–7947.
[9] H. Yu, Y. Lu, Y.G. Zhou, F.B. Wang, F.Y. He, X.H. Xia, Lab Chip 8 (2008) 1496–1501.
[10] C. Wang, S.J. Li, Z.Q. Wu, J.J. Xu, H.Y. Chen, X.H. Xia, Lab Chip 10 (2010) 639–646.
[11] (a) D. Mijatovic, J.C.T. Eijkel, A. van den Berg, Lab Chip 5 (2005) 492–500;
(b) J.L. Perry, S.G. Kandlikar, Microfluid. Nanofluid. 2 (2006) 185–193;
(c) Y. Lu, M. Wang, Chin. J. Anal. Chem. 37 (2009) 923–928.
[12] (a) M.E. Sandison, J.M. Cooper, Lab Chip 6 (2006) 1020–1025;
(b) J.O. Tegenfeldt, C. Prinz, H. Cao, R.L. Huang, R.H. Austin, S.Y. Chao, E.C. Cox, J.C. Sturm, Anal. Bioanal. Chem. 378 (2004) 1678–1692;
(c) R. Tiron, L. Mollard, O. Louveau, E. Lajoinie, J. Vac. Sci. Technol. B 25 (2007) 1147–1151;
(d) J.A. van Kan, A.A. Bettiol, F. Watt, Appl. Phys. Lett. 83 (2003) 1629–1631;
(e) K.A. Mahabadi, I. Rodriguez, S.C. Haur, J.A. van Kan, A.A. Bettiol, F. Watt, J. Micromech. Microeng. 16 (2006) 1170–1180.
[13] S.A. Gajar, M.W. Geis, J. Electrochem. Soc. 139 (1992) 2840–2883.
[14] D.S. Zhao, B. Roy, M.T. McCormick, W.G. Kuhr, S.A. Brazill, Lab Chip 3 (2003) 93–99.
[15] T. Lippert, J.T. Dickinson, Chem. Rev. 103 (2003) 453–485.
[16] P. Yang, X.X. Zhang, B. Yang, H.C. Zhao, J.C. Chen, W.T. Yang, Adv. Funct. Mater. 15 (2005) 1415–1425.
[17] R.L. McCarley, B. Vaidya, S. Wei, A.F. Smith, A.B. Patel, J. Feng, M.C. Murphy, S.A. Soper, J. Am. Chem. Soc. 127 (2005) 842–843.
[18] Y.R. Wang, H.W. Chen, Q.H. He, S.A. Soper, Electrophoresis 29 (2008) 1881–1888.
[19] S.M. Kim, M.A. Burns, E.F. Hasselbrink, Anal. Chem. 78 (2006) 4779–4785.
[20] Y. Kong, H.W. Chen, X. Yun, Z.X. Hao, Z.L. Fang, Chin. J. Anal. Chem. 35 (2007) 623–627.
[21] A. Hozumi, T. Masuda, K. Hayashi, H. Sugimura, O. Takai, T. Kameyama, Langmuir 18 (2002) 9022–9027.
[22] V. Tangpasuthadol, S.M. Pendharkar, R.C. Peterson, J. Kohn, Biomaterials 21 (2000) 2379–2387.
[23] S.J. Li, J. Li, K. Wang, C. Chen, J.J. Xu, H.Y. Chen, X.H. Xia, Q. Huo, ACS Nano 4 (2010) 6417–6424.